Flight Testing the UH-60A Airloads Aircraft

Robert M. Kufeld, Dwight L. Balough, Jeffrey L. Cross
Karen F. Studebaker, and Christopher D. Jennison
Aerospace Engineers
NASA Ames Research Center
Moffett Field, California

and

William G. Bousman
Research Scientist
U.S. Army Aeroflightdynamics Directorate (ATCOM)
Moffett Field, California

Abstract

The flight test phase of the NASA/Army UH-60A Airloads Program was completed in February 1994. The focus of the project was to measure the airloads in flight and to this purpose 221 pressure transducers were installed in nine radial arrays; plus an additional 21 transducers along the blade leading edge to better identify blade-vortex interaction phenomena. This paper briefly describes the program's background and history, instrumentation, data acquisition and processing. The database and access tools available are discussed to provide users an understanding of the capabilities for viewing the data. Data quality is examined using several different validation techniques and sample results are presented for level flight, maneuvers, and dynamic response conditions flown. A catalog of all airloads flights is included. Over 900 flight conditions were tested and half of the data have been installed in an electronic database that is accessible to industry, academia, and other government organizations. When the database is complete it will include approximately 40-60 Gigabytes of flight data.

Notation

a	speed of sound, ft/sec
a_{1c}, a_{1s}	cosine and sine 1st harmonic of flapping, deg
b	number of blades
c	blade chord, in
C_T/σ	thrust coefficient, $\frac{T}{\pi\sigma\rho\Omega^2R^4}$
C_W/σ	weight coefficient, $\frac{GW}{\pi\sigma\rho\Omega^2R^4}$
GW	aircraft gross weight, lb
l	section normal force, lb/ft
l_{TR}	main rotor/tail rotor distance, ft
L_{fuse}	fuselage lift, lb
L_{stab}	stabilator lift, lb
L_{TR}	tail rotor lift, lb
M	local Mach number
M_a	section aerodynamic moment about local quarter chord, in-lb/ft
M^2C_L	nondimensional section normal force, $\frac{2L}{a^2\rho c}$
M^2C_M	nondimensional section pitching moment, $\frac{2M_c}{a^2\rho c^2}$
M^2C_{pu}	nondimensional upper surface pressure, $\frac{2(p-p_\infty)}{a^2\rho}$
n_z	load factor, g
P	surface pressure, lb/in^2
P_∞	static pressure, lb/in^2
q	dynamic pressure, lb/in^2
Q_{MR}	main rotor shaft torque, lb-ft
Q_{TR}	tail rotor shaft torque, lb-ft
r	radial location, ft
R	blade radius, ft
SHP_{ACC}	accessory power, Hp
SHP_{ENG}	combined engine power, Hp
SHP_{INST}	instrumentation power, Hp
SHP_{MR}	main rotor power, Hp
SHP_{TR}	tail power, Hp
T	rotor thrust, lb
x	chord location, in
α_s	shaft angle of attack, deg
α_{stab}	stabilator angle of attack, deg
β	sideslip angle, deg
θ	pitch attitude, deg

Presented at the American Helicopter Society 50th Annual Forum, Washington, DC, May 11-13, 1994.

μ	advance ratio	
ρ	air density, slug/ft^3	
σ	rotor solidity,	$\frac{bc}{\pi R}$
Ω_{MR}	main rotor speed, rad/sec	
Ω_{TR}	tail rotor speed, rad/sec	

Introduction

The knowledge of the distribution of the airloads on a rotor blade in flight is fundamental to an understanding of how a helicopter works and for the design of new and improved rotorcraft. Obtaining this distribution of the airloads, however, is a difficult measurement task as it requires the installation of many pressure transducers in the blade and the acquiring and processing of the resulting pressure data. Hooper (Ref. 1), in his 1983 survey, identified ten programs where pressure measurements were obtained for at least five radial stations on the blade in either flight or wind tunnel test. Eight of these data sets[2-11] were obtained on conventional rotorcraft and two[12-13] were obtained for compound vehicles. The data obtained, particularly references 4, 5, and 9, have been very valuable in obtaining a general understanding of the complex air flow over a helicopter blade in flight and for supporting development of analysis. Despite the usefulness of these data, however, there has been a need to obtain a data set with improved bandwidth over a much greater range of flight conditions than obtained in the past.

The present program[14-16] was designed to overcome weaknesses of past programs in terms of the quality and quantity of data, the bandwidth of the data, and ease of accessibility to the data. This program is now complete and the purpose of this paper is to provide an overview of the program content and accomplishments. The paper begins with a brief discussion of the program background and how the flight tests relate to model tests already performed and wind-tunnel tests planned for the future. The rotor and aircraft instrumentation are then described. The on-board data acquisition system, which was the biggest technical challenge of the program, is described in the following section. Data processing steps to move from flight tapes to the electronic database are described as well as some of the features of the database. Examples are given of some of the data validation checks that were used and then a limited set of sample results is provided. The paper concludes with some brief remarks on what has been learned to date and work that remains to be done.

Program Background

The flight testing of the pressure-instrumented UH–60A rotor is one aspect of a larger program to obtain comprehensive measurements on a current technology rotor in flight and in the wind tunnel as well as equivalent data for a model-scale rotor. Testing has been completed for a 1:5.73-scaled UH–60A model rotor in hover[17] and in the wind tunnel[18], the present paper summarizes the flight tests of the full-scale rotor while full-scale wind tunnel testing will occur in the National Full-Scale Aerodynamic Complex (NFAC) at NASA Ames Research Center following installation and checkout of a new rotor test stand, the Large Rotor Test Apparatus (LRTA).

The start of the present flight test program dates from 1984 when an order was placed with Sikorsky Aircraft for the fabrication of two instrumented blades: a pressure blade and a blade with a mix of strain-gages and accelerometers. These blades were delivered at the end of 1988.

A first phase of UH-60A testing was instituted in a cooperative program with the U.S. Army Aviation Engineering Flight Activity at Edwards AFB as a means of proofing some of the flight test procedures to be used with the highly-instrumented rotor. These tests, completed in June 1987, used a blade with limited structural instrumentation that had been made for the U.S. Air Force's HH-60D Night Hawk program. The Phase 1 tests totaled 57 flight hours[19,20].

The second phase of the UH-60A flight test program, with the highly-instrumented blades installed, was intended to cover an extensive range of test conditions in a number of separate test campaigns. Testing, however, was delayed because of difficulties that were encountered in the development of the data acquisition system. A successful system was finally demonstrated in December 1992. In May 1993, because of severe budget cuts at NASA Ames Research Center, the test program was reduced in scope to a single test campaign. A restricted program was defined that included: (1) level flight, (2) maneuvers, (3) ground-measured acoustics, (4) airborne-measured acoustics, and (5) flight dynamics. This reduced program was started in July 1993 and was completed in February 1994. The UH-60A Airloads aircraft, shown in Figure 1, made 31 data flights during this time period for a total of 57 flight hours.

Instrumentation

Approximately 362 parameters were measured on the instrumented rotor blades and hub as outlined in Table 1 and another 93 parameters were measured on the aircraft as shown in Table 2. This section provides brief descriptions of the various sets of instrumentation. Special approaches were used to calibrate some of the instrumentation suites and, as appropriate, those calibrations are discussed here.

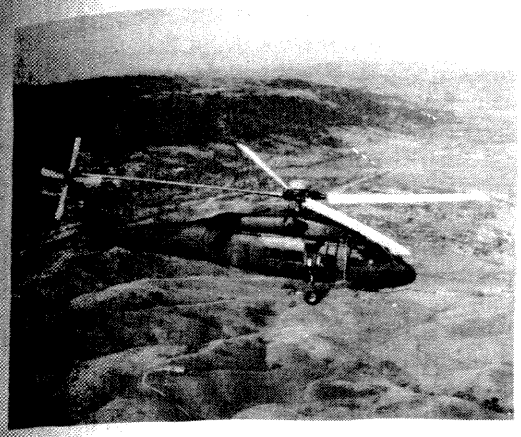

Figure 1 UH-60A with instrumented blades over the San Joaquin Valley.

Blade Pressures

The pressure blade was built with 242 sub-miniature pipette-type absolute pressure transducers[21] embedded below the skin surface of the blade. In order to maintain instrumentation integrity, the blade design specifications required that all sensors be replaceable, and that each chordwise array have spare wiring. This was accomplished with the exception of the pressure transducers inside the removable tip cap. These transducers are replaceable as a set with a spare fully pressure-instrumented tip cap. The pipettes of the pressure transducers have an outside diameter of 0.71 millimeters and are mounted flush with the airfoil sections with minimal effect on the aerodynamic flow. Blade contour measurements at each radial array have verified that the airfoil contour was not changed. The main spar of the blade was not modified during installation of transducers so as not to affect airworthiness and blade dynamics. The instrumented blade dynamic characteristics have been measured by Hamade and Kufeld (Ref. 22). Each pressure transducer has been statically calibrated over a range of 2 to 18 psia and its frequency response measured to 10,000 Hz. Most of the transducers show a flat response to 2000 Hz. The effects of temperature, centrifugal force and vibratory loading on the pressure transducers have been measured[21]. The layout of the transducers is shown in Figure 2. The spacing of the transducers was selected to allow for accurate, integrated measurements of chordwise and radial loads and to capture the most important aerodynamic phenomenon on the blade.

A unique pressure calibration technique was developed for rapid calibration of the pressure transducers after installation in the blade. A mylar sleeve is placed over the blade and both ends are sealed with a flexible sealing compound. Near the root the tube is sealed against the airfoil section of the blade itself and near the tip the sleeve is sealed against itself forming an airtight chamber. Between the blade and sleeve is a breather cloth to allow the free flow of air along the length of the blade and prevent the mylar from sealing off any of the pressure transducers. A vacuum pump and control unit is then attached to the sleeve and air is removed from the sealed sleeve to create a uniform pressure field around the blade down to 8 psi, which is the tip cap structural limit. Data is collected through the Rotating Data Acquisition System (RDAS), the

Table 1 Blade and hub rotating measurements.

Measurement Group	Number of Sensors	Sample Rate, per second	Filter Frequency, Hz
Blade Pressures	242	2142	550
Blade Temperatures	50	357	--
Blade Flap, Edge, & Torsional Moments	21	357	110
Blade Feather, Flap, & Lag Angles	12	357	110
Blade Pitch Link & Damper Load	8	357	110
Blade Flap & Edge Acceleration	20	357	110
Shaft Bending & Torque	2	357	110
Hub & Bifilar Mass Acceleration	7	357	110

Table 2 Aircraft measurements.

Measurement Group	Number of Sensors	Sample Rate, per second	Filter Frequency, Hz
Aircraft States and Controls	42	209	36
Engine States	13	209	36
Cabin Vibration Accelerometers	32	418	108
Control Loads/Tail Rotor Torque	6	836	108

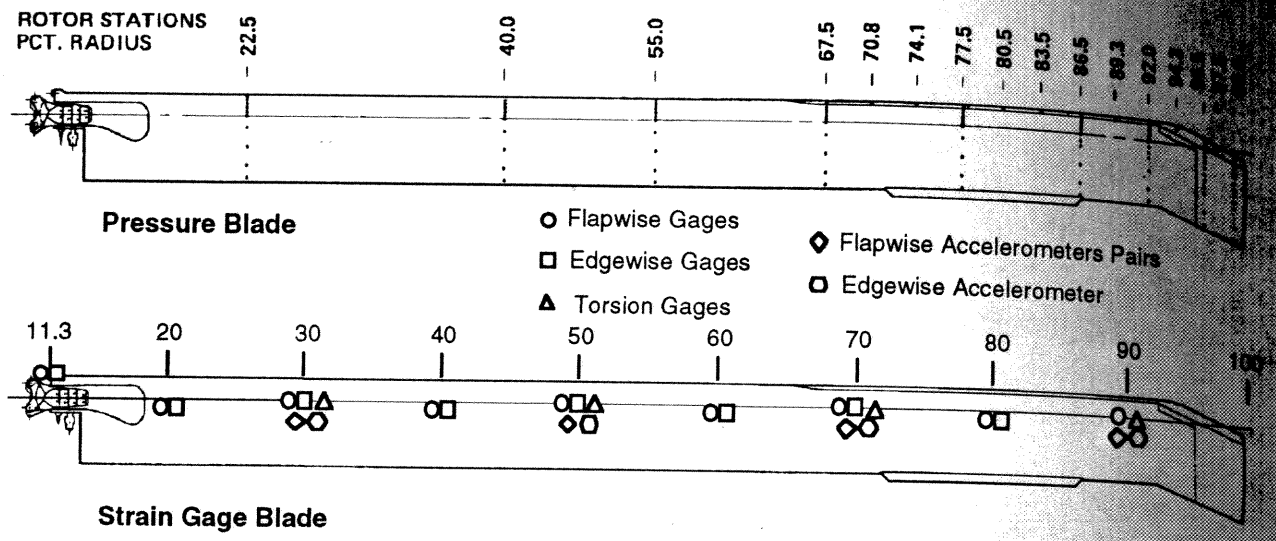

Figure 2 Schematic of pressure transducers, strain-gages and accelerometers locations along UH-60A rotor blades.

same system that is used in flight, to determine voltage gain and offset as a function of pressure. The calculated gain values are stored in a Cal File for the next series of flights. This calibration was repeated about every two to three weeks during the test program.

Blade Temperatures

Fifty pressure transducers were designed to measure blade temperature as well as pressure. These transducers were distributed in five radial arrays on both the top and bottom of the blade at 0.22R, 0.44R, 0.675R, 0.865R, and 0.965R. The temperature transducers were calibrated as installed in the blade for the range of -5° to 58° C. These temperature measurements provide the capability to correct the blade pressure for thermal effects, although this has not yet been done.

Blade Strains and Accelerations

Strain gages and accelerometers were installed in the second instrumented blade during the fabrication process. Blade flap, chord, and torsional moments were measured with a total of 21 two- or four-leg strain-gage bridges bonded directly to the spar of the blade. The measurements are evenly distributed along the blade radius as shown in Figure 2. The blade was calibrated statically with an applied load. Corrections for the blade twist distribution was made in the applied loading, but gage cross-coupling effects were assumed small and left uncorrected.

A total of twelve accelerometers were bonded to the leading and trailing edges of the spar of the strain-gage blade and were completely enclosed within the contour of the airfoil section. Eight of the twelve accelerometers measured flapwise accelerations and four measured edgewise accelerations. They are placed at four evenly spaced radial stations as shown in Figure 2. The flapwise accelerometers were installed as pairs fore and aft of the spar which allows the calculation of torsional as well as flapwise acceleration. The accelerometers were calibrated prior to installation.

Additional blade accelerometers were mounted atop each blade clevis at 0.088R and 0.125R to allow estimation of blade flapping. In addition, an accelerometer was added to each bifilar mass to measure in-plane absorber acceleration. A set of triaxial accelerometers was mounted inside the RDAS near the center of rotation to measure hub vibration. Each of these fifteen accelerometers was easily removed for laboratory calibration.

The four pitch links and dampers were instrumented with four-leg strain-gage bridges to measure axial force. The main rotor shaft extension was instrumented with two four-leg strain-gage bridges to measure shaft bending and torque. The shaft extension was calibrated at Sikorsky Aircraft's calibration laboratory using the transmission test stand prior to the flight test program.

Blade Motion Hardware

The UH–60A has a fully articulating main rotor system which incorporates an elastomeric bearing to allow independent blade flap, lag and feather motion. Because of this elastomeric bearing configuration, it is not possible to directly measure blade motion with

rotary potentiometers or similar devices. Instead, a specially designed blade motion measurement device known as the Blade Motion Hardware (BMH) was used to obtain blade flap, lag and feather measurements on each blade.

The BMH (Figure 3) uses three rotary variable differential transformers (RVDTs) to measure rotations which approximate blade flap, lag and feather motions. Since the BMH is not located at the blade hinge point, the RVDT outputs measure coupled blade motions. The true blade motions are obtained through three kinematic equations which account for the blade coupling. The kinematic equations for each blade include ten coefficients that must be determined by calibration. The calibration procedure begins by adjusting pitch and roll of the aircraft using hydraulic jacks until the main rotor shaft is in the vertical position. The pitch link of the blade to be calibrated is then positioned over the forward primary servo to allow maximum blade feather deflection. A sighting transit is then mounted on top of the RDAS, directly above the main rotor shaft centerline, using a specially designed fixture. The sighting transit is used to determine the lead-lag position of the blade relative to the hinge point using simple geometry. Blade flap and feather motions are measured with a digital inclinometer placed at the blade root.

Aircraft State Measurements

The aircraft state measurements include airspeeds; angular attitudes, rates, and accelerations; linear accelerations; and angle of attack and sideslip from vanes mounted on the test boom. The airspeed measurements are obtained by three independent airspeed measurement systems: one installed in the test boom, the aircraft system, and the Helicopter Air Data System (HADS). The boom and aircraft measurements are used for airspeeds above approximately 30 knots. The HADS is used to obtain airspeed data below 30 knots. All three systems were calibrated using a ground pace vehicle for speeds below 60 knots. However, analysis of the HADS calibration data yielded poor results. A second calibration using the ground laser tracking system at speeds ranging from 40 knots forward to 10 knots rearward was performed, however, the data from this calibration have not been analyzed at this time. The boom and aircraft systems were calibrated at higher speeds using a T–34 pace aircraft.

Fuselage Vibration

There were 35 fuselage accelerometers mounted in the aircraft measuring lateral, longitudinal, and vertical accelerations. Vibration was measured in the cockpit and cabin, and on the transmission, cabin absorber, tail, and stabilator. The sensor locations match those of a ground vibration test conducted on a different UH–60A vehicle configured similarly to the Airloads aircraft[23].

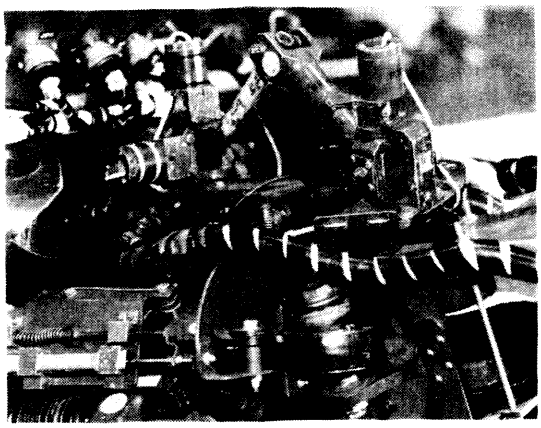

Figure 3 UH–60A Blade Motion Hardware.

Flight Controls

The flight control positions were measured using conventional displacement transducers such as potentiometers and linear variable differential transformers (LVDTs). In addition to the pilot control positions, the control mixer inputs, the Stability Augmentation System (SAS) actuator positions, and the flight control servo positions were also measured. Control position calibration was standard except for the SAS actuators which were calibrated by injecting a hardover signal into the flight control computer with a signal generator box provided by Sikorsky Aircraft.

Engine States

Engine state measurements were obtained from standard instrumentation provided by the engine manufacturer except for the fuel flow measurements. The fuel flow measurements were provided by separate turbine-type meters installed in the fuel lines.

Data Acquisition

Flight data from the UH-60A Airloads aircraft were obtained with two airborne data acquisition systems. For a limited number of tests, ground-based tracking data were also obtained and merged with the aircraft data. The first system, the Rotating Data Acquisition System (RDAS), was mounted atop the rotor hub and collected data from main rotor sensors. The second system, the Airframe Data Acquisition System (ADAS) was mounted inside the cabin and collected data from non-rotating components plus RDAS and ADAS health monitoring information. The main RDAS and ADAS measurement groups are summarized in Tables 1 and 2, and these include the sample rates and filter frequencies.

Rotating Data Acquisition System (RDAS)

The RDAS was designed around ten identical Pulse Code Modulation (PCM) encoders and has a system data bit rate of 7.5 megabits per second. Data sampling is controlled by a common synchronization pulse sent to

all ten encoders from a timing card inside the RDAS. Each encoder has been programmed in an identical manner collecting 35 ten-bit main frame words, which include time code, rotor position and run counter data to ensure data synchronization. The ten-bit encoders provide a useful range of 1000 counts for analog inputs and 1024 counts for bi-level (digital) inputs. The maximum encoder bit rate of 750 kilobits per second provides 2142.86 samples per second for each main frame parameter. Five of the main frame words were set up in a six deep sub-commutation configuration providing a lower sample rate of 357.14 samples per second for 180 sensors, which included blade temperatures, blade moments, pitch link and damper loads, blade accelerations and motions.

Analog data from transducers mounted on the blades, pitch links, dampers, and the rotor hub were passed through either 550 or 110 Hz six-pole Butterworth filters and gain amplifiers to sample and hold amplifiers. The analog signals were then digitized by the ten encoders and were stored as a digital stream. The ten digital data streams were then sent down through a slip ring into the aircraft cabin.

Inside the cabin, the ten streams were inspected for valid encoder signals and were then combined by a multiplexer into a single 7.5 megabit per second stream. Before multiplexing, data from any of the ten streams could be telemetered to the ground station for real time monitoring. This signal was then routed through a digital spreader unit which divides the data stream into nine tracks, each with an alignment tag, which were then recorded onto a fourteen track Frequency Modulation (FM) tape recorder. This step was necessary as FM tape recorder technology does not reliably handle this high data rate. Upon post-flight data processing, discussed below, the nine data streams were re-merged with the help of the alignment tags into the single 7.5 megabit stream.

Inside the RDAS (Figure 4) there were forty identical signal conditioning cards which provided space for filters and gain amplifiers for 320 transducers. The gain and offset of each transducer (with the exception of temperature measurements) were controlled by high precision resistors that were soldered to the signal conditioning cards. Each resistor was specifically selected to obtain the optimal match with that channel's transducer output. This enabled the 10-bit RDAS system to deliver an average resolution of 0.026 psi per count for the pressure transducers. This method of gain and offset control was used because it provided a low sensitivity to temperature variation and could better withstand the high dynamic loads of the rotating hub in flight.

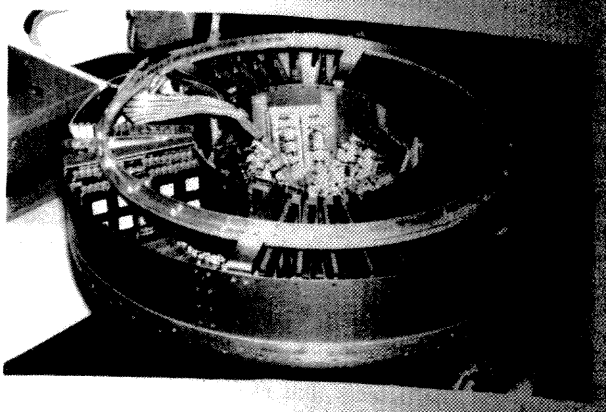

Figure 4 View of signal conditioning cards and encoders inside the RDAS.

The RDAS was developed and built at Ames Research Center and represents a major step forward in "state-of-the-art" flight data acquisition hardware. The operation of this system in a helicopter flight environment was one of the biggest risks undertaken by this program. The high reliability of the RDAS throughout the flight program was a key element in the program's success.

Airframe Data Acquisition System(ADAS)

The ADAS acquired data from all non-rotating measurements, including aircraft and engine states, control positions, and system health monitoring parameters. In contrast to the 10-bit PCM encoders used in the RDAS, the ADAS incorporated 12-bit PCM encoders. The 12-bit encoders provided a useful range of 4000 counts for analog inputs and 4096 counts for bi-level (digital) inputs. The system dynamic range was approximately 72 dB.

The ADAS featured adjustable system gain to allow compatibility with a variety of sensor output voltage levels. The PCM encoder gain was variable from 0.5 to 20, while the gain of the signal conditioning modules was limited to 1, 8 and 250. Unlike the RDAS, these gains were programmable and did not require resistor changes. The product of the encoder gain and the signal conditioning gain yielded the effective system gain for a particular measurement. However, encoder gain greater than unity was found to increase system noise and thus only signal conditioning gain was used for most measurements. In certain cases, the sensor excitation voltage was modified (within the linear range of the device) to achieve the desired measurement resolution.

As installed in the UH-60A Airloads aircraft, the ADAS had three anti-aliasing filter modules available. These three filters had -3 dB points at approximately 36,

72 and 108 Hz. The PCM bit map was designed to provide a minimum sample rate of four times the filter cutoff frequency. The nominal sample rates for the low mid, and high-rate parameters were: 209, 418, and 836 samples per second. As configured for this test, the ADAS could acquire data from up to 115 individual measurements.

Ground-Based Flight Path Tracking

A ground-based laser and radar tracking system was used during the fly-over acoustic testing, low speed testing, and the hover flight dynamics tests at NAS Crows Landing. The tracking data were merged with a select group of aircraft state parameters that were telemetered to the ground. These data were recorded into a digital database as compressed, tagged data. This format has long been a standard at NASA Ames for flight data, and has been reprocessed into the keyed access database used for all aircraft data.

The aircraft had a laser reflector cube installed on each landing gear fairing to allow tracking with a pulsed Nd:YAG laser tracker. The laser tracker has an average accuracy of 1 ft at one standard deviation out to 30,000 ft and 2 ft at two standard deviations beyond that distance.

The radar tracking system was used in conduction with the laser tracker and was used as a back-up if the laser return signal was not satisfactory. The radar system consists of two modified Nike Hercules X-Band monopulse radar trackers that lock on to a transponder mounted in the aircraft or were capable, with reduced accuracy, of tracking from the aircraft reflection. The radar tracker had an average accuracy of 7 ft. at one sigma out to 15000 ft, and 7 feet plus 1 % at distances out to 60,000 ft. The system has an azimuthal accuracy of 0.3 milliradians at one sigma.

Flight Test Procedures

Under normal procedures each test flight was launched from NASA Ames Research Center at Moffett Field. An initial housekeeping point was taken in an OGE hover at Moffett and then the aircraft, accompanied by a chase aircraft, was flown to the San Joaquin Valley in the vicinity of NAS Crows Landing where reduced air traffic allowed for productive flight testing. Enroute a second housekeeping point was taken at an 80-knot indicated airspeed and 1000-ft altitude. One of the ten RDAS encoder streams and the ADAS data stream were telemetered to the ground station at Moffett Field to be monitored on strip charts and CRT displays. For flights requiring specific test conditions, such as a constant C_W/σ, calculations were made in the Test Director's Workstation and the aircraft was directed to an appropriate altitude. A screwjack-actuated ballast cart was installed in the aircraft and this was positioned by the Flight Test Engineer to maintain a constant center of gravity for the aircraft as fuel was burned off. At the completion of the test card the aircraft returned to Ames Research Center and, if sufficient tape remained in the tape recorders, the outbound housekeeping points were repeated. Normally, one flight was performed on a test day, but if two flights were made the aircraft landed at NAS Crows Landing and re-fueled.

During the ground-measured acoustics portion of the program, the aircraft was stationed in Modesto in the San Joaquin Valley to reduce flight time to Crows where the ground acoustic array was located. Although telemetry monitoring continued at the ground station at Moffett Field during this phase, the flight test was controlled from the instrumentation vans at Crows.

Data Reduction

Data reduction or processing consisted of a number of steps for each counter (data point) and these steps were performed by two separate organizations: the Ground Data Center and the TRENDS Database Manager. For a normal counter, normalized plots of aircraft speed, attitudes, C_W/σ, and several other parameters were calculated real time by the Test Director's Workstation using telemetered data. These plots were used to determine the best contiguous five seconds of data for post-flight processing. This process, called time slicing, was completed prior to the arrival of the flight tape at the Ground Data Center.

The next step in the reduction process was calibration processing. A data file, called the Cal File, was computed for each transducer for each flight. The scale values in the Cal File were determined from laboratory calibrations or bag calibrations for the various parameters and, in most cases, were first order or linear calibrations. In a few cases, higher order fits were used and stored in the Cal File. Parameter offsets were determined for most parameters by a process called Calibration Equivalence. In this process, counters that contain the pre- and post-flight static records were used to determine an average PCM count and this was equated to a pre-set engineering value. This equivalence was then used to set the offset or bias term for all flight counters. For the pressure transducers, as an example, the pre-set engineering value was the static pressure that was measured at the aircraft prior to flight.

Once the initial time slicing and calibration processing was complete, the data were read from the flight tape and stored as compressed, tagged time history data files. Statistics using the raw counts were calculated for fast initial data access and automated quality checks were performed for band edge, spikes, and dead transducers. The compressed, tagged data files were transferred to the TRENDS Database Manager for

reformatting into the interactive keyed access format used by the data access software, as discussed below. Reformatting was done on a counter-by-counter basis and was a function of the length of each counter. Then, statistics and derived parameters were computed from the time history files. The data was initially stored on magnetic disk while being reviewed for correctness. After completion of an engineering review the data were transferred to an optical disk for permanent storage.

Typically, only five seconds of a 20-second steady-flight condition were time sliced and archived in the database because of storage limitations. For maneuvers or dynamic conditions, data were processed and stored in files that were up to 45 seconds long. Optical disk storage was the limiting factor for these cases. If a counter was longer than 45 seconds, it was divided into two, three, or four different counters that were appended together as required by end users and no data are lost during this process.

Derived Parameters

There were many parameters of interest that cannot be directly measured but could be derived from measured data. Seventy-one such parameters have been included in the database obtained during the flight research portion of the UH-60A Airloads Program. These parameters are summarized in Table 3 and are discussed below.

Table 3 Derived parameter groups and numbers.

Derived Parameters Group	Number of Parameters
Aircraft c.g. linear acceleration	3
True and calibrated airspeeds	11
Tail rotor and engine corrected shaft torque	4
Engine shaft horsepower	4
Main and tail rotor shaft horsepower	3
Corrected blade motion	12
Atmospheric ratios	3
Dimensional and non dimensional states	10
Ground tracking position and speed	18
Miscellaneous	3

In the case of the aircraft center-of-gravity (c.g.) accelerometers, it was impossible to locate the accelerometers at the exact c.g., therefore, the data were corrected using measured angular data. The calibrated and true airspeed for the instrumentation boom and ship system as well as the low speed air data sensor were computed based on the calibration flight data.

The tail rotor torque was measured from the tail rotor drive shaft, prior to the intermediate gear box. Since this rotates at a higher speed than the tail rotor, the computed torque is adjusted to compensate for the speed change. Derived parameters are included for the shaft horsepower of both engines individually and combined, main and tail rotors individually and combined, and shaft horsepower loss.

The Blade Motion Hardware measurements are cross coupled and are converted to true root displacements with a set of kinematic equations. Density, pressure and temperature ratios are included in the database based on aircraft measured temperature and pressure.

Flight research involves testing to nondimensional conditions such as coefficients of gross weight, thrust and power, advance ratio, and advancing tip Mach number. These nondimensional parameters along with dimensional quantities such as aircraft c.g. and gross weight are included in the database as derived parameters.

Finally, for cases where laser and radar tracking data were obtained these data were converted to a runway reference system.

Data Access

The data from the UH–60A airloads flight test were stored in the TRENDS database for fast and easy access. In addition to the flight data and derived parameters, the database also contains additional descriptive material and measurements that complement the flight data. The various types of data are discussed below.

Flight Test Data

The measured time history files are stored as 16-bit integer words. Conversion to engineering units is performed when the user plots or reads out the data. This allows the user the option of querying the database for the raw data in counts as well as engineering units and this has proven to be valuable during the data validation stage of the program. Derived parameter time histories, as described previously, are stored as real values in engineering units which requires twice the storage space.

At the time that the flight data were installed in the database and the derived parameters were created, two

additional sets of data were computed and stored: (1) statistical properties of the data, and (2) harmonics of the data. The additional data sets were computed for a subset of parameters, primarily loads, blade moments, and accelerometer data. The statistical properties have been most useful during the development flight program leading to airworthiness release of the aircraft.

Narrative Data

The database includes narrative data relevant to the flight test program. Included in the narrative data are: (1) brief descriptions of each flight, (2) one line descriptions of each flight counter, (3) descriptions of sensors, and (4) descriptions of derived parameters. A number of software tools are available that can be used to search the counter descriptions and the flight data so as to create sets of flight counters that meet specified search criteria[24,25].

Calibration Data

Calibration files are also accessible in the database and these provide a history of the gain and offset values used over the flight test program.

Data Analysis and Management Tools

Two software packages are available that access the common keyed access database: the Tilt Rotor ENgineering Database System (TRENDS)[24,25] and the Data from Aeromechanics Test and Analytics Management and Analysis Package (DATAMAP)[26-29]. TRENDS was developed to support the XV-15 flight research program and has been enhanced to handle the UH-60A Airloads database. DATAMAP was developed under U.S. Army auspices to support the AH-1G Operational Loads Survey[9] airloads study. It has been upgraded by NASA to support the Tip Aerodynamics and Acoustics Test[10,11] and now the Black Hawk Airloads Program[20].

The TRENDS software includes two separate packages. The first, the Data Base Management package, is a suite of programs that process data into the database. The second, the Analysis Applications package, allows the user to access, manipulate, search, display and export the data interactively. It handles all of the various data types such as statistics, narrative, and time histories. It is menu driven and operates as a question and answer session. It is a good general analysis tool, although it is not intended to support airloads analysis. A number of the plots presented in this paper were generated using TRENDS.

DATAMAP includes both data analysis and data management capabilities, however for this application, only its analysis capabilities are used. DATAMAP accesses only the time history database with a user interface using detailed command steps to specify the actions to be employed from the available suite of analysis and derivation options. The derivations include pressure coefficients and normal, edgewise, and pitching moment coefficients. DATAMAP has an extensive plotting capability, can export data, and although it is usually run interactively, it can be run in batch mode.

A third program, Plot/DataBase (P/DB), is also used to analyze the data and operates with batch command files. P/DB, strictly a data analysis tool, was developed to support the analysis of the many published airload databases. It therefore reads data files stored as ASCII time history, or harmonic tables. In order for it to access the UH-60A Airloads database, the specific counter and sensors of interest must be exported from the keyed access database using either TRENDS or DATAMAP. The resulting ASCII data files are very large, and data management is a user responsibility. It duplicates many of the functions that DATAMAP encompasses plus includes many unique features. Many of the data plots presented in this paper were generated using the P/DB.

Data Validation

A number of approaches have been used to demonstrate the validity of the data obtained during the UH-60A flight test program. The majority of these approaches are based upon some form of internal consistency check, that is, comparing one type of measurement with another. These checks can vary from simple parameter-to-parameter comparisons to more elaborate checks that require extensive calculation. The following sections discuss a number of these validation checks.

Pitch-link Load Replication

A straightforward consistency check is the comparison of measurements made on different blades. Figure 5 shows the pitch-link load measurements obtained on the four blades as a function of blade azimuth and cycle count at maximum speed in level flight. For this level speed point nineteen complete cycles or revolutions of data were recorded and, in this figure, each cycle is plotted adjacent to the previous cycle. The surface plots for each pitch link provide a qualitative assessment of the loading behavior. In general, the four pitch links are very similar, showing the most positive loading in the first quadrant, a rapid reduction in loading in the second quadrant and then, on the retreating side of the disk, two cycles of a 4/rev oscillation. Small blade-to-blade differences are seen in these figures as well, both in higher harmonic content and in the steady amplitude. The small differences at higher frequencies may in fact represent small blade-to-blade differences while the differences in steady pitch-link load level are believed to be a result of the differences in trim tab settings required for blade tracking.

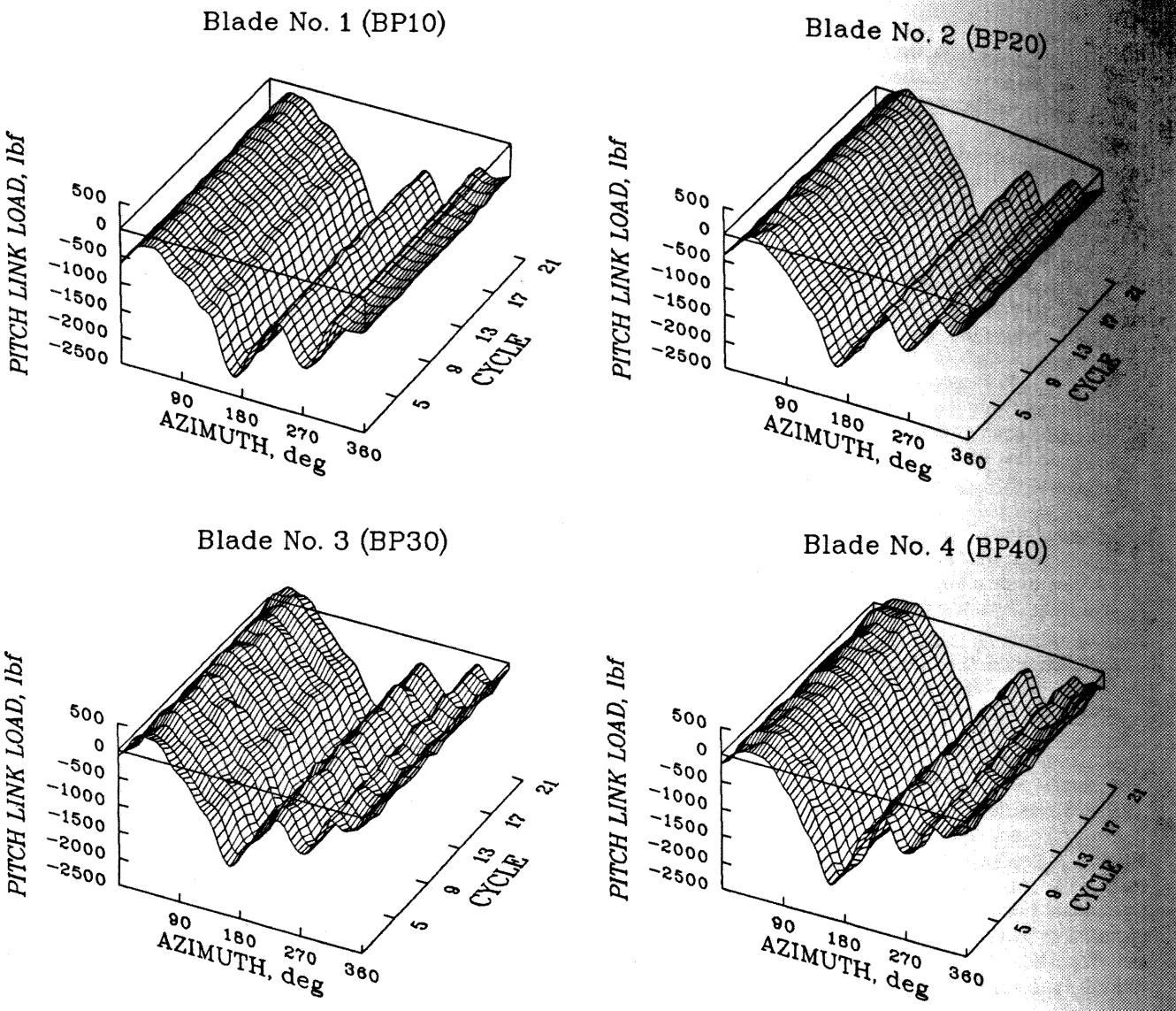

Figure 5. Pitch-link load as a function of blade azimuth and cycle number for four blades (Counter 8534); C_W/σ = 0.08, μ = 0.368, 0–12 harmonics.

The good agreement that is shown in Figure 5 is encouraging. However, it is recognized that such agreement is only a necessary condition for data validity and not a sufficient condition as there are a number of potential systematic errors that could equally affect the four measurements shown here. Although the point of this figure is to show the consistency between measurements it is also useful to note the steadiness of the data as evidenced by the small cycle-to-cycle variation, particularly for blades one and two.

Power Balance

A second consistency check is the comparison of the power measured by sensors on the engine output shafts with measurements of main rotor and tail rotor shaft torque. The expected power balance is

$$SHP_{ENG} = SHP_{MR} + SHP_{TR} + SHP_{ACC} + SHP_{INST} \quad (1)$$

where

$$SHP_{MR} = Q_{MR}\Omega_{MR}/0.97 \quad (2)$$

$$SHP_{TR} = Q_{TR}\Omega_{TR}/0.98 \quad (3)$$

The accessory power (SHP_{ACC}) is not measured directly, but the test instrumentation power (SHP_{INST})

is. The main rotor gearbox is assumed to have 97% efficiency, the tail rotor gearbox 98% efficiency and the tail rotor torque measurement is obtained on the drive shaft prior to the intermediate gearbox.

Figure 6 compares the measured rotor torques converted to power at the engines with the measured engine power at the output shafts. The data were obtained on Flight 83 and are particularly useful for this comparison as test points were obtained at flat pitch on the ground as well as at maximum level flight speed conditions. The accessory and instrumentation power are not included with the main and tail rotor power values in this figure. Assuming that the accessory and instrumentation powers do not vary with airspeed, then a curve fitted to the data should have a slope of one. For this flight the slope is 0.974 indicating a difference of -2.6%. The offset represents the accessory and instrumentation powers and the average value is 74 Hp. If lower transmission efficiencies are assumed, for example, 95% efficiency for both main and tail rotor, the slope is 0.995 and the offset is 44 Hp.

Flapping Trim

The blade 1/rev flapping angles and the 1/rev bending moment on the main rotor shaft are separate measurements of the trim moments of the aircraft in flight. In the absence of 1/rev shears at the hub center these two sets of measurements should show good agreement. Flight 83 includes a series of tests on the ground with the rotor collective set to flat pitch and with 1-inch control inputs in the lateral and longitudinal control axes. Figure 7 compares the calculated shaft bending moment based on measured and estimated 1/rev flapping angles with the measured shaft bending moment. The calculated shaft bending moments are based on a centrifugal force at the elastomeric bearing[30] of 70,853 lb. Solid and open square symbols show the moments based on the flapping angle measurements

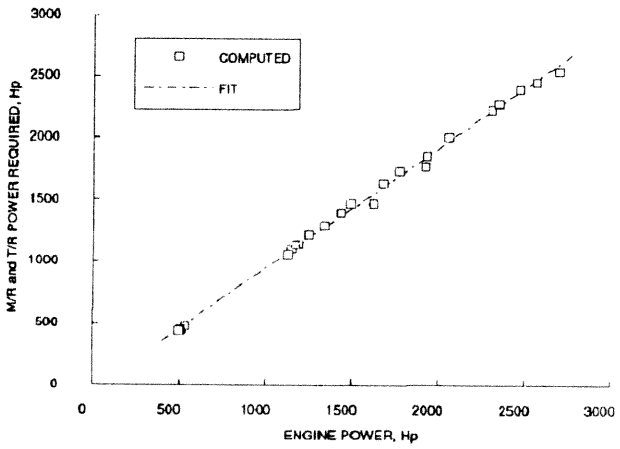

Figure 6. Measured main rotor and tail rotor power (at the engine output shaft) compared with measured engine power for Flight 83.

while the X shows the shaft bending moment based on flap angle estimates[31] obtained from blade accelerometers mounted on the inner portion of the blade at 0.088R and 0.125R. Compared to a slope of unity the shaft bending based on blade 1 flapping measurement is 5.2% low, shaft bending based on the blade 3 flapping measurement is 1.8% low, and based on the blade 3 flapping estimate 1.4% low. Although not shown here the phase agreement of these measurements are equally good. The mutual validation of these different measures of aircraft trim are encouraging and any of the three should be suitable as a specification of trim.

Thrust Balance

A force-balance check that is unique to this aircraft is to compare the integrated airloads on the blade with the forces on the aircraft. The approximate force balance equation in the vertical direction is

$$T \cong GW - L_{fuse} - L_{stab} - L_{TR} \qquad (4)$$

GW is the aircraft gross weight and is continuously updated based on the initial weight of the aircraft with corrections for fuel burned. The fuselage lift is based on 0.25-scale wind tunnel tests[32] and, for level flight

$$L_{fuse} = 1.66q\theta \qquad (5)$$

where q is the dynamic pressure and θ is the pitch attitude. The stabilator lift is based on the measured angle of attack of the stabilator, α_{stab}, as well

$$L_{stab} = 1.78q(\theta + \alpha_{stab}) \qquad (6)$$

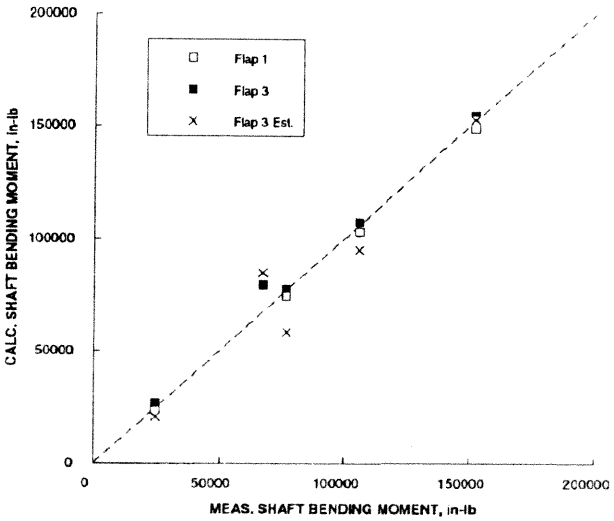

Figure 7. Calculated 1/rev shaft bending moment based on flapping angles compared with measured 1/rev shaft bending moment (Counters 8311 to 8315).

while the lift caused by the tail rotor is approximated based on main rotor torque as

$$L_{TR} = (Q_{MR}/l_{TR} - 0.83q\beta)\tan 20° \quad (7)$$

and the distance of the tail rotor from the main rotor, l_{TR}, is 32.565 ft and tan20° accounts for the canted tail rotor on the Black Hawk. The horizontal and vertical stabilizer lift coefficients have also been obtained from Ref. 32. It is noted that the effect of sideslip on the tail rotor lift is very small in level flight.

The blade thrust was obtained from the section normal force by a simple, trapezoidal spanwise integration. Blade twist was neglected in the integration and the influence of shaft tilt was also neglected. The two sides of the force balance equation are compared in Figure 8 where the integrated thrust values are shown as open squares and the gross weight adjusted for fuselage, stabilator, and tail rotor lift is shown as a solid line. Above an advance ratio of about 0.1 the integrated pressures are about 7% high and the cause of this is not known. Below $\mu = 0.1$ the aerodynamic corrections to the gross weight are no longer important and the major difference between thrust and gross weight is the rotor wake induced download which is not accounted for here.

The overprediction of the blade pressures refers, of course, to the steady component and it is this steady component which is most difficult to measure correctly. More work needs to be done to examine the effects of temperature corrections to the pressure offset terms as well as more precise calculations of the integrated thrust. The integrated blade thrust follows the expected trend with airspeed very well and the scatter appears to be on the order of two to three percent.

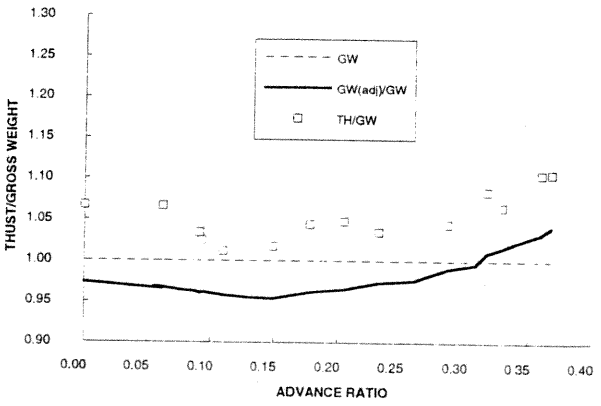

Figure 8. Comparison of thrust-to-gross-weight for measured aerodynamic loads (open squares) and adjusted gross weight (solid line) as a function of advance ratio: Flight 85.

Blade Response to Airloads Comparison

A check of the blade airloads that provide ... assessment of the unsteady airloads is to use ... measured airloads in a forced response calculation ... and compare the calculated blade bending moments ... measured moments. The calculation method, ... Response to Aerodynamic Loads (BRAL), solves ... equations of motion using a differential equation solver. For the calculations shown here, the problem was treated as an uncoupled flap response problem and, therefore, neglected coupling effects with the chord degree of freedom and the lead-lag damper at the blade root. The measured flapping response is compared with the calculated response in Figure 9 where the flap bending moment is shown on a surface plot as a function of blade azimuth and radial station. There is

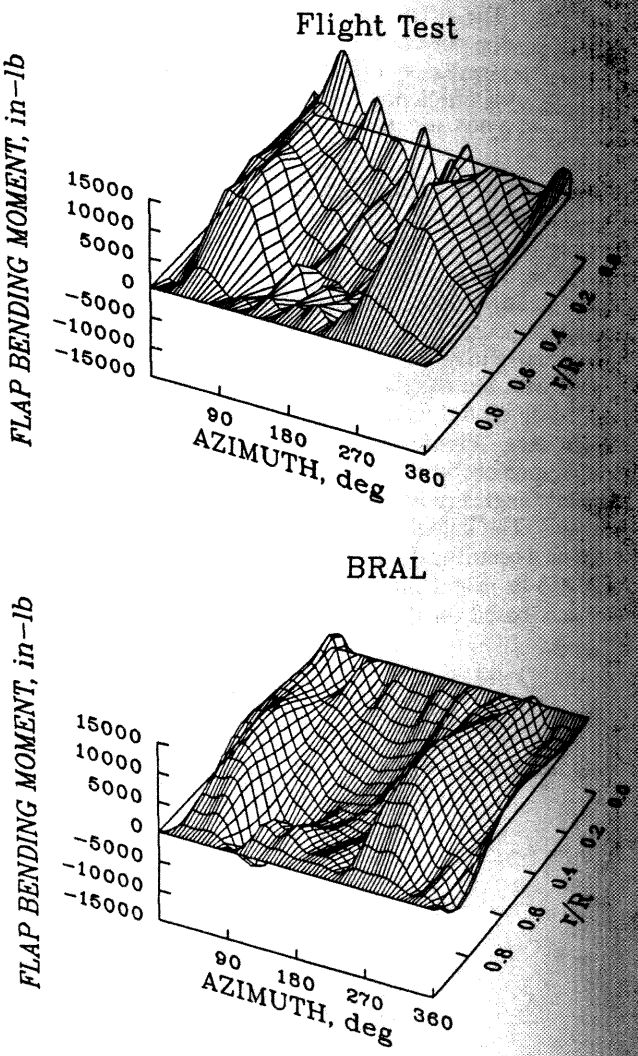

Figure 9. Comparison of blade flapping moments measured in flight test with flapping moments calculated from measured airloads (Counter 8534); $C_W/\sigma = 0.08$, $\mu = 0.368$, 0–12 harmonics.

good qualitative agreement, especially towards the blade tip, between the measured flap bending moments and those calculated from measured airloads and, as these two sets of measurements are completely independent, the agreement validates both sets. The BRAL calculation does not show the higher harmonic loading that is seen inboard on the blade and this may be a consequence of the uncoupled calculation. Similar behavior was shown in Ref. 33. The measured flap bending moment amplitudes near midspan are higher than those calculated by BRAL and the reasons for this are not known.

Model-Scale Test

The consistency checks that have been discussed in this section are all internal checks in that portions of the data are compared with other portions. An external check that is of considerable interest is to compare measurements in flight test with experimental measurements obtained in a test of a 1:5.73-scale UH-60A model in the DNW wind tunnel[18]. Trim values are shown for a set of paired test conditions in Table 4. Differences between the flight test and wind tunnel test include: (1) scale effects, particularly Reynolds number effects, and design features associated with model scale construction; (2) flapping trim is based on zero harmonic flapping in the wind tunnel; (3) flow angularity in the wind tunnel is sensitive to the shear layer; (4) thrust trim is based on aircraft weight in flight and on the balance in the wind tunnel; (5) rotor inflow effects induced by the aircraft fuselage in flight are not present in the wind tunnel; and (6) data processing differences: averaged data are shown for the wind tunnel and a single cycle is shown for the flight data. The thrust trim, item (4), is probably least important in this case as the fuselage lift, stabilator lift, and tail rotor lift are approximately in balance at $\mu = 0.30$ so that the rotor thrust and aircraft weight are approximately the same; see Figure 8.

The section normal forces are compared for the two test conditions in Figure 10. The normal force is shown as a function of blade azimuth and radial station. Qualitatively, the two sets of data are similar, however, there is more negative lift near the blade tip for the wind tunnel point and the negative lift extends over a greater range of azimuths. The distribution of normal force shows a number of small differences both radially and azimuthally. In addition, there are small differences seen on both the advancing and retreating sides of the rotor near the tip that are caused by vortices trailed from the previous blades.

Table 4. Trim Conditions for Flight and Wind Tunnel Test.

Parameter	Flight Test (8424)	Wind Tunnel (Run 13, Pt 10)
C_T/σ	0.089	0.087
μ	0.304	0.301
a_{1c}	1.31	0.10
a_{1s}	1.33	0.05
α_s	-4.32	-4.49

The differences in the vortex induced loading are examined in more detail in Figure 11 where the section normal forces at 0.965R are compared. This figure clearly shows the greater negative lift in the second quadrant for the model rotor and phase differences in loading caused by the vorticity from previous blades. In

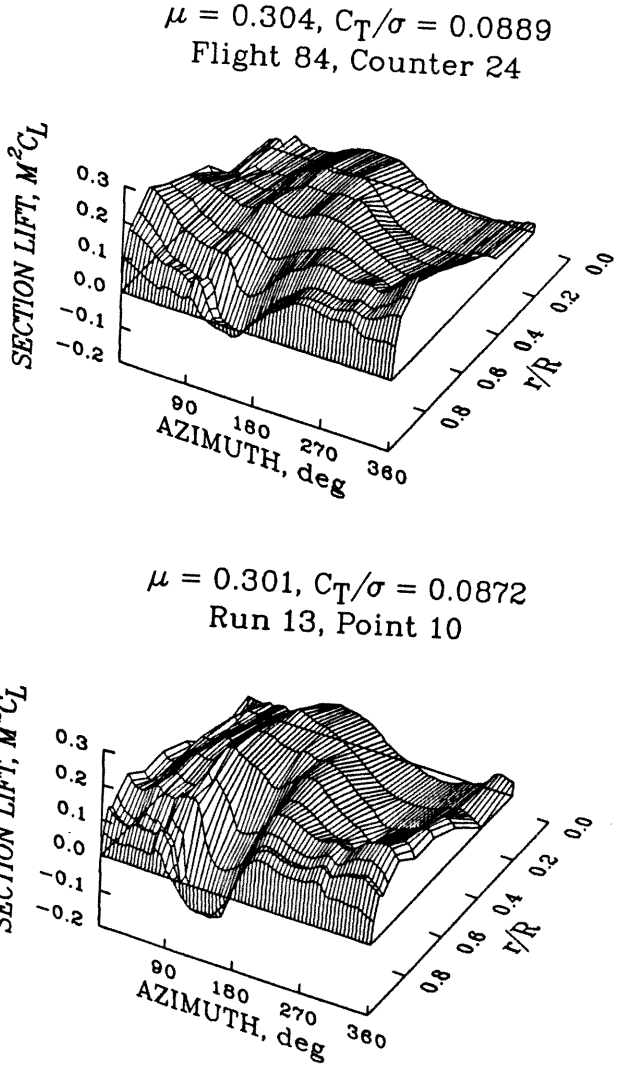

Figure 10. Comparison of section lift measured in flight and in the wind tunnel as a function of blade azimuth and radial station.

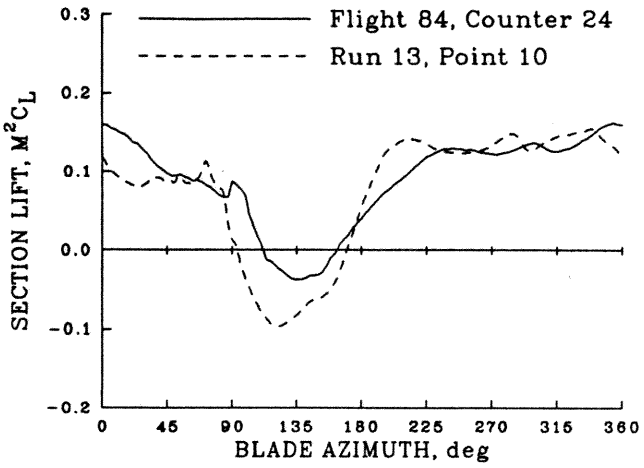

Figure 11. Comparison of section lift measured in flight and in the wind tunnel as a function of blade azimuth; r/R = 0.965.

general, there is considerable agreement between the two data sets and this helps to validate the flight test data. At the same time, the differences shown here are important for the issue of scaling of test data and offer interesting research opportunies.

Sample Results

Flight test data have been obtained for a large number of test conditions. As discuss previously these test conditions can be roughly categorized as (1) level flight, (2) maneuver, (3) ground-measured acoustics, (4) flight-measured acoustics, and (5) flight dynamics. A flight catalog is included in the appendix to serve as a guide to these test conditions. This section will provide sample results for these test conditions except for the acoustic tests which were performed in cooperation with Langley Research Center (ground-measured acoustics) and the NFAC at Ames Research Center (flight-measured acoustics) as these will be reported elsewhere. The various examples shown here are meant only as a brief introduction to this large of the flight test database.

Level Flight

Steady, level flight, airspeed sweeps were flown for six values of C_W/σ to provide baseline airloads data that show the effects of advance ratio and blade loading[35]. The limiting condition in each level flight sweep was the 30-minute engine power limit. Figure 12 shows the evolution of the airloads at 0.92R, just inboard of where the blade sweep starts. This surface plot shows the nondimensional section lift as a function of blade azimuth and advance ratio. Advance ratio varies from 0.093 to 0.368 and each advance ratio line on the surface plot represents a separate test condition. At low

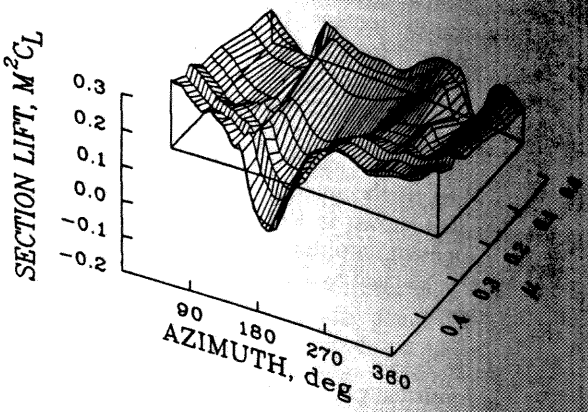

Figure 12. Section lift as a function of blade azimuth and advance ratio; $C_W/\sigma = 0.08$, r/R = 0.92, 0–60 harmonics.

speeds the influence of vorticity loading from the tip vorticies of previous blades is clearly evident on the advancing side of the disk where there is a down-up pulse and on the retreating side where there is an up-down pulse. This vorticity loading peaks at an advance ratio of about 0.1 and, of course, is the source of the high vibratory loading that is observed in transition flight. As advance ratio increases the loading caused by the tip vortices diminishes, but its influence is still visible on this plot beyond an advance ratio of 0.3. The character of the section lift changes as advance ratio increases so that the lift is reduced in the second quadrant to maintain roll moment balance on the aircraft[1]. At this radial station the lift is negative for advance ratios beyond 0.20. The basic loading shown here appears typical for rotors in forward flight[36].

The blade airloads at the highest speed condition in Figure 12 are shown in Figure 13 as a function of blade azimuth and radial station. Each line on the surface plot represents the integrated normal force at a particular radial station from the most inboard station at 0.225R to the most outboard at 0.99R. The section lift at 1.00R is, of course, zero. At the most inboard station on the rotor the lift is largest over the nose of the aircraft and then decreases rapidly and becomes negative in the third and fourth quadrants because of reverse flow. Moving out on the blade the lift is positive in all quadrants and tends to concentrate over the fore and aft portions of the rotor disk. A section of reduced loading develops in the second quadrant because of the need to maintain roll-moment balance and the lift is zero at 0.775R for this airspeed. The region of negative lift in the second quadrant is greatest at 0.92R and is reduced as the blade tip is approached. This behavior is very similar to the lift distributions examined by Hooper in his classic study[1].

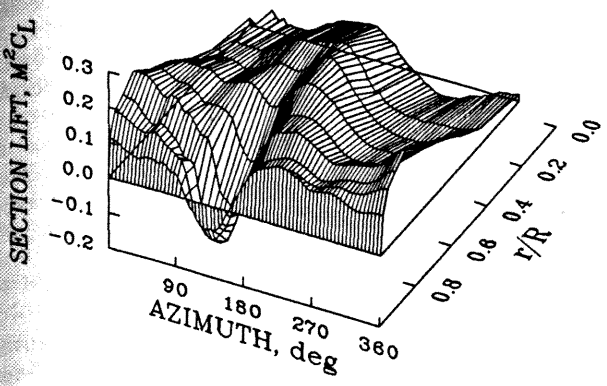

Figure 13. Section lift as a function of blade azimuth and radial station (Counter 8534); $C_W/\sigma = 0.08$, $\mu = 0.368$, 0–60 harmonics.

Figure 14 compares the frequency response of the blade in the flapwise direction with hub vertical acceleration for the first twenty rotor harmonics for the data shown in Figure 13. The flapwise response in Figure 14a was measured by an accelerometer at fifty percent blade radius. The strong peak at 3/rev is a result of the 2nd flapwise mode at 2.87/rev. Figure 14b shows the vertical response at the rotor hub. The rotor harmonics combine and cancel at the hub leaving predominantly 2 and 4/rev. The large response at 12/rev is the first vertical mode of the RDAS which was measured in a shake test and predicted using finite element analysis. It is unusual that Fig 14b shows non-integer responses above and below n/rev[37]. This phenomenon may be explained by Floquet's theorem which predicts that blade dissimilarities cause additional peaks in the frequency spectrum[38]. The UH–60A Airloads aircraft does have slight dynamic dissimilarities in the blades as was shown in a ground vibration test[22]. These differences are due to small mass and stiffness differences of the instrumented blades; however, the blades are a matched set that have been tracked and balanced to a master blade.

The data shown in Figures 12 and 13 are from the first cycle (revolution) of the test condition record. As each condition is held for approximately five seconds, this means that the record contains approximately 19 or 20 revolutions or cycles of data. Coleman and Bousman[35] have demonstrated the steadiness of these data for level flight cases by showing the time histories of a pressure transducer on the lower surface as a shock passes over the transducer for the high-speed test condition of Figure 13. Figure 15 shows a similar plot for a pressure transducer on the upper surface. In this figure the nondimensional pressure is shown as a

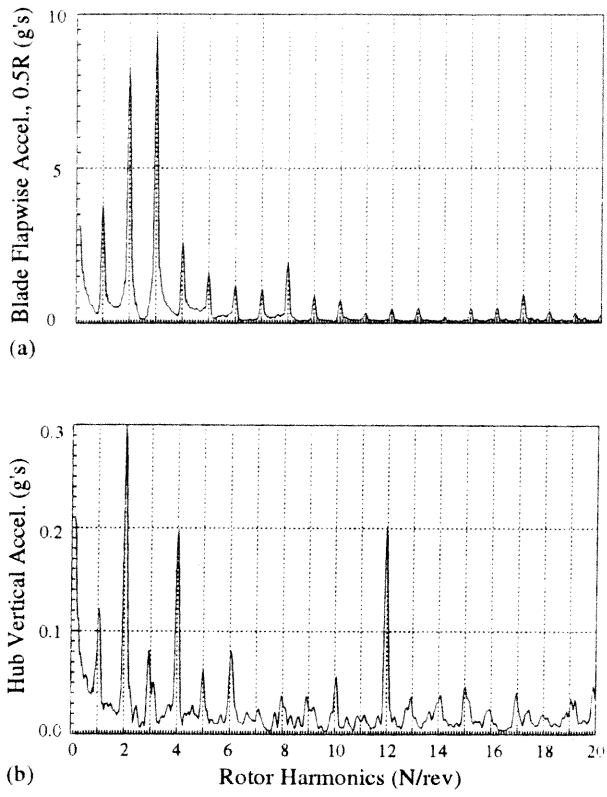

Figure 14a and b. Frequency responses of the 0.5R blade flapwise and hub vertical accelerations in level flight (Counter 8534); $C_W/\sigma=0.80$, $\mu=0.368$.

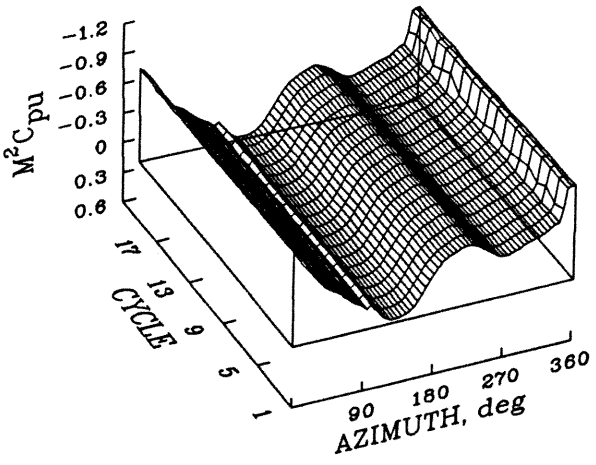

Figure 15. Upper surface pressure as a function of blade azimuth and cycle number (Counter 8534); x/c = 0.030, r/R = 0.865, C_W/σ = 0.08, μ = 0.368, 0–60 harmonics.

function of blade azimuth and cycle count. Steadiness in the data is evidenced by the smoothness of the surface. For the case shown here two different phenomena are seen for this transducer near the leading edge of the airfoil. First, just at the start of the second quadrant, a small change in pressure is observed which appears to be caused by a small vortex, perhaps from the previous blade. The loading from this vortex or vortex-like pressure change has little effect on the overall blade loading, but it is interesting to observe how steady and repeatable this phenomenon is. A much stronger change in pressure is seen at the end of the fourth quadrant where a shock passes over the transducer location. The shock is quite strong during this initial passage as the angle of attack is quite high over the aft portion of the disk. As the blade enters the first quadrant the angle of attack is decreasing very rapidly and the area of supercritical flow is reduced such that the returning shock is never observed at this location. Despite the rapid variation in angle of attack around the rotor disk and the resulting strong pressure gradients, the figure shows that the data are very steady over the entire length of the record. Only a slight unsteadiness is seen during the pressure drop associated with the shock passage.

In some cases the airloads are noticeably unsteady over the five-second period of a test condition. For the highest loading condition, $C_W/\sigma = 0.13$, the rotor undergoes two dynamic stall cycles[35] at the limiting forward speed of $\mu = 0.236$. During these stall cycles there is considerable unsteadiness in the airloads as well as elastic motion in the rotor. Figure 16 shows the nondimensional section moment at 0.865R for this case

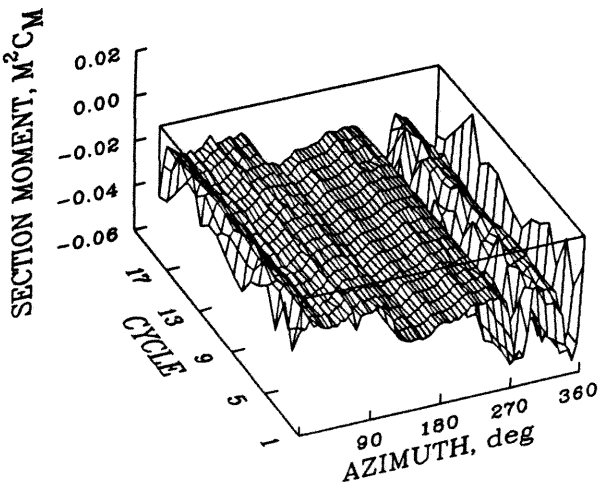

Figure 16. Section pitching moment as a function of blade azimuth and cycle number (Counter 9017); r/R = 0.865, $C_W/\sigma = 0.13$, $\mu = 0.236$, 0–60 harmonics.

as a function of blade azimuth and cycle count. The section pitching moment is relatively stable in the first three quadrants of the rotor, but then considerable unsteadiness is observed over the two dynamic stall cycles starting just prior to 270 degrees and finishing near the beginning of the first quadrant. The average loading in this case will represent a good test of dynamic stall models, but the unsteadiness that is seen in this figure also represents information that may be important in the understanding of the dynamic stall mechanisms.

Flight Maneuvers

Data have been obtained for a variety of maneuvers during the flight test program including pull-ups, pushovers, roll-reversals, rolling pullouts, steady turns, wind-up turns, settling with power. An understanding of the aerodynamic loads during maneuvers is important as these loads frequently size the rotor and flight controls.

One of the sample results examined here shows a portion of a pull-up and a pushover maneuver[39]. In both of these maneuvers the pilot flies a roller coaster-like flight path. As an example, Figure 17 shows the stick inputs and pitch response for a pull-up maneuver that results in a period of reduced g flight as the aircraft is pitched over into a dive and then rapidly pulled out of the dive to develop the target load factor. Note that in this maneuver, the longitudinal SAS is saturated during

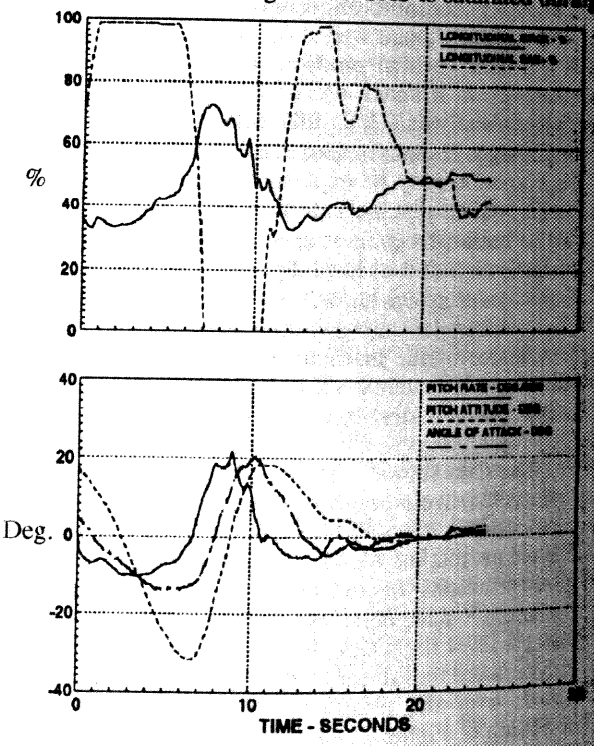

Figure 17 Longitudinal stick input, SAS response, pitch attitude, pitch rate, and angle of attack for a pull-up maneuver (counter 8927).

the severest portion of the maneuver. The pushover maneuver is very similar in that the aircraft is pitched up and develops a load factor greater than one, and then it pitches over and the targeted reduced load factor is achieved.

The first maneuver examined here is the high load factor portion of a 0.25-g pushover where a load factor of 1.71g was obtained for four revolutions of the rotor. The nondimensional section lift at 0.865R is shown in Figure 18 for the four rotor revolutions. Little variation is seen in the section lift over this time period, and in this sense, the maneuver can be considered a steady maneuver. The rotor thrust in this case is equivalent to steady flight at $C_W/\sigma = 0.13$, but unlike the steady flight case[35] no stall occurs in the third and fourth quadrant of the disk. In addition the effects of multiple blade vortex intersections are observed in the first quadrant of the disk; this is an effect not observed in level flight.

In contrast to the steady maneuver data of Figure 18, Figure 19 shows the section lift during an unsteady maneuver. These data, taken in a pull-up just prior to reaching the target load factor, show every other revolution from a point at approximately 1.0g (Cycle 32) to a load factor of 2.0g (Cycle 40). The section lift essentially doubles over the course of this maneuver and a variety of blade vortex intersections are observed on both the retreating and advancing sides of the disk during the course of the maneuver.

On two occasions at the lower end of a level flight speed sweep, the aircraft entered the flight condition known as 'settling with power'. The first counter was flown at C_W/σ=0.09, while the second counter of settling with power was flown at C_W/σ=0.11. The condition was not encountered during the other C_W/σ speed sweeps.

Figure 20 presents the altitude, rate of climb, and collective stick position for the first of these points. The target test point had been level flight at 15 knots, however as the aircraft approached this condition it began to settle with power. It can be seen that the pilot increased collective on two occasions but the inputs did not arrest the rate of descent. The climb rate shown is derived from filtered static pressure data.

The aircraft state data for this 'settling with power' condition when compared to the nearest level fight condition at $C_W/\sigma = 0.08$, revealed that the main rotor torque, pitch attitude, and control positions were all very similar. An examination of the blade forces shows very little difference when compared with a similar level flight case and the details of this flight condition require further investigation.

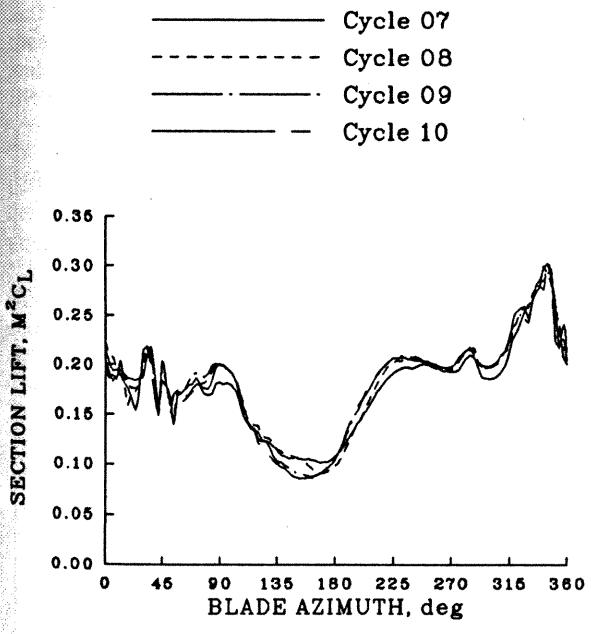

Figure 18. Section lift as a function of blade azimuth during a period of steady load factor during a pushover maneuver (Counter 8930); r/R = 0.865, n_z = 1.7g, μ = 0.236, 0–60 harmonics.

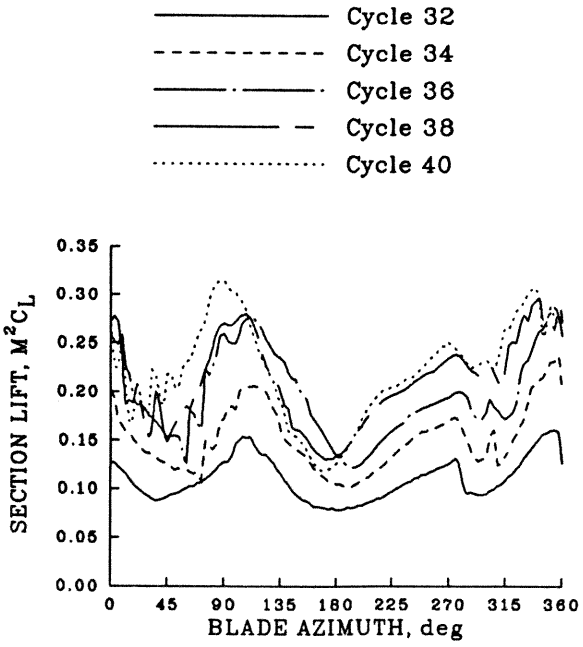

Figure 19. Section lift as a function of blade azimuth as n_z varies from 1.0g to 2.0g in a pull-up maneuver (Counter 8927); r/R = 0.865, μ = 0.230, 0–60 harmonics.

Flight Dynamics

Frequency sweep testing or the use of specific control motions to excite the lower frequency motion of the aircraft is an important approach to identifying aircraft models and using these models to design improved flight control systems. The UH–60A Airloads aircraft provided a unique opportunity to obtain these kinds of data while simultaneously measuring the blade airloads. Figure 21a shows the vertical response of the aircraft c.g. during a longitudinal frequency sweep input at 70 knots. The longitudinal stick position for the same maneuver is shown in Figure 21b. Both the vertical response and the longitudinal control input have been filtered at 10 Hz to remove 4/rev vibratory components. The gradual build-up of the control from low frequency to high frequency is evident in Figure 21b. The frequency of the initial control is approximately 0.1 Hz. The maximum frequency of the control input is approximately 6 Hz and is reached 85 seconds into the maneuver. A modal amplification of the vertical response is clearly evident in Figure 21a as the input approaches 6 Hz. This mode is believed to be the fuselage first vertical bending mode. Pre-flight predictions[40] using the NASTRAN finite element model estimated the natural frequency of the fuselage first vertical bending mode at 6.322 Hz. The frequency sweep input was terminated after the bending mode was encountered.

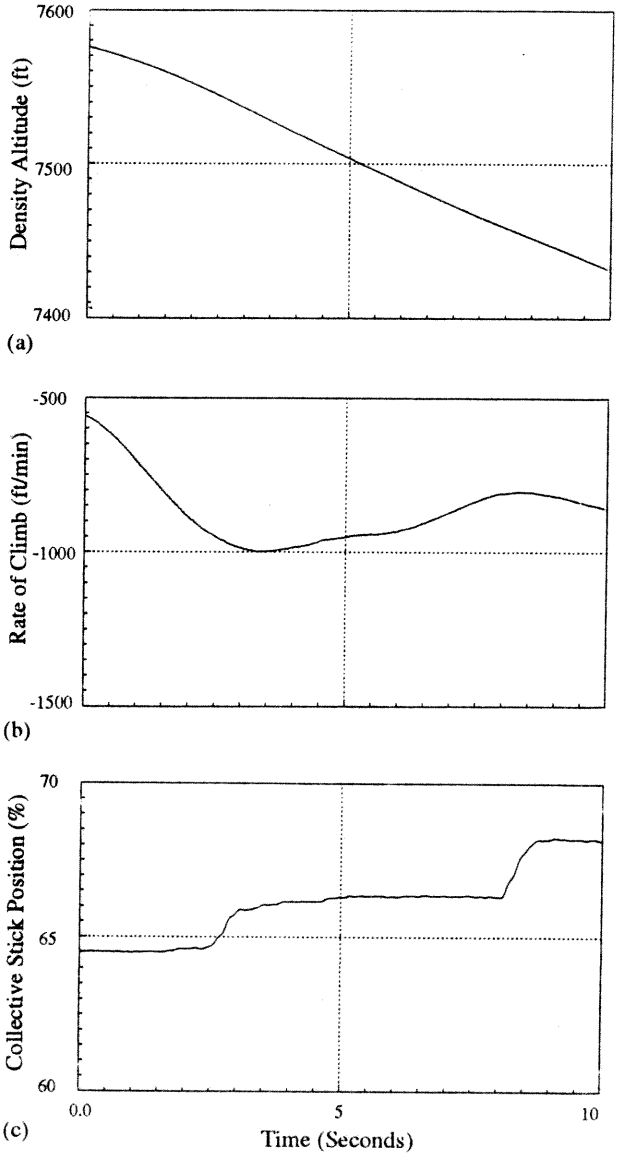

Fig 20 Altitude, climb rate, and collective vs time for settling with power test condition, (Counter 8421); C_W/σ=0.09.

Concluding Remarks

The airloads flight test of the UH-60A Airloads Project, started in 1984, has been completed. The present paper has provided an overview of the instrumentation, the data acquisition and data processing, example data validation checks, and some sample results. The most technologically challenging aspect of the program was the on-board data acquisition system which with its long development cycle became the pacing item in the scheduling of the flight research.

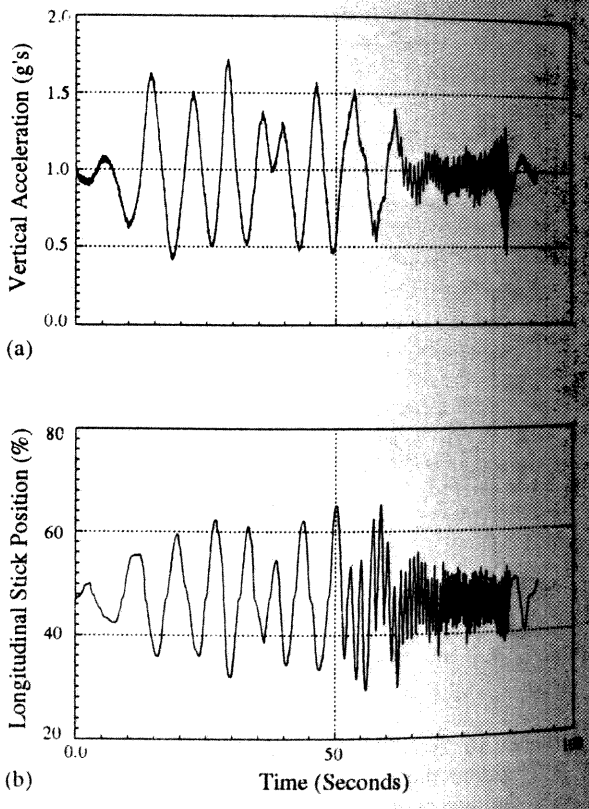

Figure 21a and b. UH-60A vertical acceleration and longitudinal control position during longitudinal frequency sweep input at 70 kts.

As shown here, most of the data acquisition problems were overcome and the data are, in general, of good quality. At this time only about half of the data acquired in the flight program are in the database and considerable work remains in processing the remaining flight tapes, assuring the quality of the data, and providing the data in a useful form to the industry, academia, and other government organizations.

Acknowledgments

The flight test program described in this paper was accomplished through the efforts of many people, from instrumentation designers, to acquisition system designers, instrumentation engineers, electronics technicians, mechanics, airworthiness engineers, inspectors, pilots, flight support personnel of all varieties, computer programmers, and many more. All of these people worked as a team and all performed superbly. Special acknowledgment is made of the project pilots, Rick Simmons and Munro Dearing, for their steady flying and continuous support, and the former Program Manager Ed Seto, who retired before the airloads flight testing began.

A number of organizations at NASA and the US Army provided assistance when data were first obtained with the system and their aid in this crucial phase was invaluable. Tom Norman is acknowledged for his steadfast help with the pressure data review. Chee Tung and Mark Silva also assisted in this area plus brought their experience with the DNW data to assist the team, and Tom Maier is acknowledged for his work with BRAL and his quiet counsel.

Significant portions of the flight test program were performed cooperatively with other organizations and their assistance and expertise was invaluable. The ground-measured acoustics program was done with NASA Langley Research Center and Arnold Mueller. His joint NASA-Army team are acknowledged for their dedicated efforts under a very difficult schedule. The airborne-measured acoustics was done with personnel from the NFAC at NASA Ames, and Dave Signor and his team are acknowledged. Finally, Jay Fletcher of the US Army, is acknowledged for his assistance with all of the flight dynamic testing.

References

1. Hooper, W. E., "The Vibratory Airloading of Helicopter Rotors," *Vertica*, Vol. 8, No. 2, 1984, pp. 73-92.

2. Rabbott, J. P. and Churchill, G. B., "Experimental Investigation of the Aerodynamic Loading on a Helicopter Rotor Blade in Forward Flight," NACA RM L56107, 1956.

3. Burpo, F., "Measurements of Dynamic Airloads on a Full-Scale Semi-Rigid Rotor," TCREC TR 62–42, 1962.

4. Scheiman, James, "A Tabulation of Helicopter Rotor-Blade Differential Pressures, Stresses, and Motions as Measured in Flight," NASA TM X–952, 1964.

5. Rabbott, J. P., Jr., Lizak, A. A., and Paglino, V. M., "A Presentation of Measured and Calculated Full-Scale Rotor Blade Aerodynamic and Structural Loads," USAAVLABS TR 66–31, 1966.

6. Rabbott, J. P., Jr., Lizak, A. A., and Paglino, V. M., "Tabulated CH-34 Blade Surface Pressures Measured at NASA/Ames Full Scale Wind Tunnel," SER–58399, December 1965.

7. Pruyn, R. R., "In-Flight Measurement of Rotor Blade Airloads, Bending Moments, and Motions, Together with Rotor Shaft Loads and Fuselage Vibration, On a Tandem Rotor Helicopter," USAAVLABS TR 67–9A, 1967.

8. Beno, Edward A., "CH–53A Main Rotor and Stabilizer Vibratory Airloads and Forces," SER 65593, June 1970.

9. Shockey, Gerald A., Cox, Charles R., and Williamson, Joe W., "AH–1G Helicopter Aerodynamic and Structural Loads Survey," USAAMRDL TR 76–39, 1977.

10. Cross, Jeffrey L. and Watts, Michael E., "Tip Aerodynamics and Acoustics Test," NASA RP 1179, December 1988.

11. Cross, Jeffrey L. and Tu, Wilson, "Tabulation of Data from the Tip Aerodynamics and Acoustics Test," NASA TM 102280, November 1990.

12. Bartsch, E. A., "In-Flight Measurement and Correlation with Theory of Blade Airloads and Responses on the XH-51A Compound Helicopter Rotor, Volume I Measurement and Data Reduction of Airloads and Structural Loads," USAAVLABS TR 68–28A, 1968.

13. Fenaughty, Ronald and Beno, Edward, " NH–3A Vibratory Airloads and Vibratory Rotor Loads," SER 611493, January 1970.

14. Watts, Michael E. and Cross, Jeffrey L., "The NASA Modern Technology Rotors Program," AIAA 3rd Flight Test Conference, 1986.

15. Snyder, W., Cross, J, Kufeld, R, "NASA/ Army Rotor Systems Flight Research Leading to the UH-60A Airloads Program", Presented at AHS Specialists Meeting, Innovation in Rotorcraft Test Technologies, October, 1990.

16. Kufeld, R. and Loschke, P, "UH-60 Airloads Program: Status and Plans," AIAA Aircraft Design, Systems, and Operations Meeting, September 1991.

17. Lorber, Peter F., Stauter, R. Charles, and Landgrebe, Anton J., "A Comprehensive Hover Test of the Airloads and Airflow of an Extensively Instrumented Model Helicopter Rotor," American Helicopter Society 45th Annual Forum Proceedings, May 1989, pp. 281–295.

18. Lorber, Peter F., "Aerodynamic Results of a Pressure-Instrumented Model Rotor Test at the DNW," Journal of the American Helicopter Society, Vol. 36, No. 4, October 1991, pp. 66–76.

19. Buckanin, Robert M., Gould, Warren, Losier, Paul W., Downey, David A., Lockwood, Roy, Webre, James L., Hagan, John F., Cason, Randall W., and Young, Christopher J., "Rotor Systems Evaluation, Phase I," AEFA Project No. 85–15, March 1988.

20. Cross, J., Brilla, J., Kufeld, R., and Balough, D., "The Modern Rotor Aerodynamic Limits Survey: A Report and Data Survey," NASA TM 4446, October 1993.

21. Gagnon, R., "Sub-Miniature Sensor Installation for UH-60A Main Rotor Blade Air Loads Flight Test Program," Presented at the International Telemetry Conference, 1989.

22. Hamade, K. and Kufeld, R., "Modal Analysis of UH–60A Instrumented Rotor Blades", NASA TM 4239, November 1990.

23. Durno, J. A., Howland, G. R., and Twomey, W., "Comparison of Black Hawk Shake Test Results with NASTRAN Finite Element Analysis," American Helicopter Society 43rd Annual Forum Proceedings, May 1987, pp. 511–526.

24. Bjorkman W. and Bondi M., "TRENDS: The Aeronautical Post-Test, Database Management System", NASA TM-101025, January 1990.

25. Bondi M. and Bjorkman W., "TRENDS: A Flight Test Relational Database Users Reference Manual", NASA TM-108806.

26. Philbrick R., "The Data from Aeromechanics Test and Analytics – Data Management Package, Volume One – Users Manual", USAAVRADCOM-TR–80–D–30A, December 1980.

27. Philbrick R., "The Data from Aeromechanics Test and Analytics – Data Management Package, Volume Two – System Manual", USAAVRADCOM-TR–80–D–30B, Dec. 1980.

28. Watts M., Dejpure S., "DATAMAP Upgrade Version 4.0", NASA TM-100993, March 1989.

29. Chase J., "DATAMAP Grammer, A Description of the New User Interface Command Parsing Methodology". Sterling Software, Inc., TN-93-8825-000-1, June 1993.

30. Bousman, William G. and Maier, Thomas H., "An Investigation of Helicopter Rotor Blade Flap Vibratory Loads," American Helicopter Society 48th Annual Forum Proceedings, June 1992, pp. 977–999.

31. Balough, Dwight L., "Estimation of Rotor Flapping Response Using Blade-Mounted Accelerometers," American Helicopter Society Aeromechanics Specialists Conference, January 1994.

32. Barnard R., "YUH-60A/T700 IR Suppressor Full Scale Prototype Test Report," SER70094, June 1976.

33. Esculier, Jacques and Bousman, William G., "Calculation and Measured Blade Response on a Full-Scale Rotor," Journal of the American Helicopter Society, Vol. 33, No.1, January 1988, pp. 3–16.

34. Maier, Thomas H., "An Examination of Helicopter Rotor Load Calculations," American Helicopter Society National Specialists' Meeting on Rotorcraft Dynamics, November 1989.

35. Coleman, Colin P. and Bousman, William G., "Aerodynamic Limitations of the UH-60A Rotor," American Helicopter Society Aeromechanics Specialists Conference, January 1994.

36. Bousman, William G., "The Response of Helicopter Rotors to Vibratory Airloads," Journal of the American Helicopter Society, Vol. 35, No. 4, October 1990, pp. 53-62.

37. Studebaker, K., "A Survey of Hub Vibration for the UH–60A Airloads Research Aircraft," presented at the American Helicopter Society Aeromechanics Specialists Conference, January, 1994.

38. McNulty, M. J., "Effects of Blade-To-Blade Dissimilarities on Rotor-Body Lead-Lag Dynamics,"

presented at the Eleventh European Rotorcraft Forum, London, England, September 1985.

39. Kufeld, Robert M., Cross, Jeffrey L., and Bousman, William G., "A Survey of Rotor Loads Distribution In Maneuvering Flight," American Helicopter Society Aeromechanics Specialists Conference, January 1994.

40. Idosor, F. R., and Seible, F., "NASTRAN Modeling of Flight Test Components for UH60A Airloads Program Test Configuration," Univ. of California, San Diego Report No. SSRP - 93/03, February 1993.